Measurement of holmium Rydberg series through magneto-optical trap depletion spectroscopy

J. Hostetter,* J. D. Pritchard, J. E. Lawler, and M. Saffman†
Department of Physics, University of Wisconsin-Madison, 1150 University Avenue, Madison, Wisconsin 53706, USA
(Received 3 December 2014; published 16 January 2015)

We report measurements of the absolute excitation frequencies of ^{165}Ho $4f^{11}6sns$ and $4f^{11}6snd$ odd-parity Rydberg series. The states are detected through depletion of a magneto-optical trap via a two-photon excitation scheme. Measurements of 162 Rydberg levels in the range $n = 40$–101 yield quantum defects well described by the Rydberg-Ritz formula. We observe a strong perturbation in the ns series around $n = 51$ due to an unidentified interloper at 48515.47(4) cm^{-1}. From the series convergence, we determine the first ionization potential $E_{IP} = 48565.910(3)$ cm^{-1}, which is three orders of magnitude more accurate than previous work. This work is an important step towards using Ho atoms for collective encoding of a quantum register.

DOI: 10.1103/PhysRevA.91.012507 PACS number(s): 32.10.Fn, 32.30.Jc, 32.80.Ee

I. INTRODUCTION

Rydberg atoms have been studied extensively, yielding important information about atomic structure and ionization thresholds [1,2]. Rydberg atoms are attracting intense current interest in the area of quantum-information processing due to their strong dipole-dipole interactions [3]. The Rydberg dipole blockade provides a strong, switchable interaction between neutral atoms, allowing for the creation of quantum gates and entanglement [4]. Two-qubit gates have so far been demonstrated in the alkali atoms rubidium [5,6] and cesium [7]. There is further interest in using the Rydberg blockade in ensembles of atoms to create a collectively encoded quantum register [4,8]. Collective encoding is most beneficial in atoms with a large number of ground hyperfine states [9]. The stable atom with the largest number of hyperfine ground states is holmium. Its nuclear spin is $I = 7/2$ and the electronic angular momentum of the ground state is $J = 15/2$, providing 128 hyperfine ground states with total angular momentum $F = 4$–11. The large angular momentum arises due to the open $4f$ shell in the ground-state electronic configuration. As with other rare-earth elements, this open-shell structure results in an extremely complex energy spectrum that is challenging to reproduce theoretically due to strong relativistic effects and configuration interactions [10]. For Rydberg atom quantum-information processing, knowledge of the Rydberg levels is important for accurate prediction of the dipole-dipole interaction strengths and sensitivity to external fields.

Studies of the Rydberg spectra of neutral rare-earth elements have been limited to date, with initial measurements of the ionization potentials for the full range of lanthanides [11] and actinides [12] and energy-resolved Rydberg states for La [13], Eu [14], Dy [15], Lu [16], Gd [17], Sm [18], Th [19], Ce [20], Yb [21], Ac [22], Pu [23], and U [24]. In this paper we present high-resolution spectroscopy of the $4f^{11}6sns$ and $4f^{11}6snd$ odd-parity Rydberg states of Ho in the range $n = 40$–101 using depletion measurements on a magneto-optical trap (MOT). The resulting spectra are used to extract accurate values for the first ionization potential and quantum defects for the series, in addition to revealing a strong perturbation around $51s$ which is analyzed in the framework of multichannel quantum defect theory (MQDT). Additionally, we observe a previously unpublished repumper transition from a metastable state giving significant enhancement in the MOT atom number. These measurements provide important information about the fundamental atomic structure of the open-shell configuration for testing against *ab initio* models.

II. EXPERIMENTAL SETUP

Depletion spectroscopy is performed using two-photon excitation with ∼100 kHz linewidth lasers of a Ho MOT via the strong $4f^{11}(4I^{\circ}_{15/2})6s6p(^1P^{\circ}_1)$ cooling transition, with a radiative linewidth of $\gamma/2\pi = 32$ MHz. The experimental setup, shown schematically in Fig. 1(a), uses the apparatus detailed in Ref. [25]. An atomic beam of Ho is slowed using a 400-mW counterpropagating beam, derived from a frequency-doubled Ti:sapphire laser, which is detuned in the range of −210 to −330 MHz from the $4f^{11}(4I^{\circ})6s^2, F = 11$ to $4f^{11}(4I^{\circ}_{15/2})6s6p(^1P^{o}_1), F' = 12$ transition at 410.5 nm. Atoms are loaded into a MOT formed at the intersection of three pairs of orthogonal beams with a detuning of −20 MHz and a total power of 400 mW, resulting in a saturation parameter of $I/I_{sat} = 1.06$. The equilibrium atom number is 7.5×10^5 at a temperature <500 μK, with a density of 2.2×10^{10} cm^{-3}.

The MOT population is measured using a photodiode to monitor fluorescence. The collected fluorescence signal is amplitude modulated with an optical chopper, followed by lock-in detection, to suppress background electronic noise. At the two-photon resonance, atoms are excited to Rydberg states leading to increased loss of the MOT from decay into dark states and photoionization of the Rydberg atoms, reducing the equilibrium number. For each measurement, spectra are averaged over 50 repetitions, and increasing and decreasing frequency ramps of the 413-nm laser are compared to verify that resonances are observed in both scan directions as well as to account for any hysteresis in the frequency ramp.

The MOT cooling laser is stabilized to an ultra-high-finesse ultra-low-expansion (ULE) reference cavity ($\mathcal{F} \sim 2 \times 10^5$) mounted in vacuum and temperature controlled to <±10 mK, providing <1 MHz frequency drift for several weeks of measurements. The short-term laser linewidth after locking to the reference cavity is estimated to be ∼100 kHz.

*hostetter@wisc.edu
†msaffman@wisc.edu

 ©2015 American Physical Society

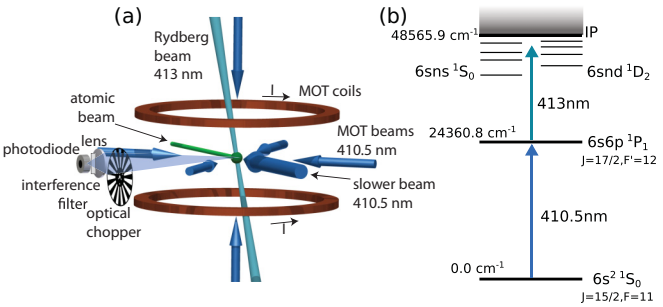

FIG. 1. (Color online) Experimental setup. (a) A focused Rydberg excitation laser is overlapped with a Ho MOT, resulting in depletion of the equilibrium atom number on resonance. (b) Energy-level diagram: Rydberg atoms are created through two-photon excitation via $6s6p\,^1P_1\,F' = 12$, with the first photon provided by the 410.5-nm MOT beams.

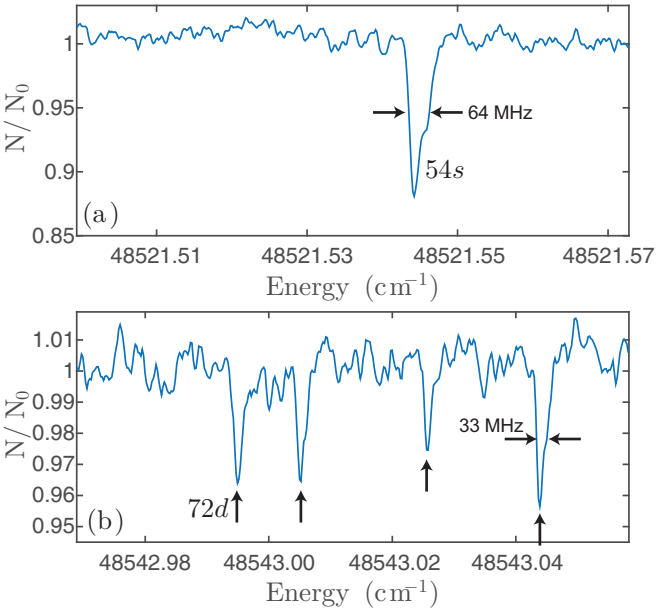

FIG. 2. (Color online) MOT depletion spectra. (a) Isolated depletion line for the $54s$ state, resolved with a 60-MHz full width at half maximum (FWHM). (b) Multiple fine-structure states are resolved for the $72d$ series, with the lowest energy level used to determine the series parameters as it is typically the strongest resolved line for each n.

Rydberg excitation is achieved using a frequency-doubled 826-nm diode laser producing 3 mW at 413 nm, which is focused to a waist of 27 μm and overlapped on the MOT. The 826-nm laser is locked to a Fabry-Pérot reference cavity and scanned across 1–2 GHz with a scan period of about 10 s using the cavity piezo. The Fabry-Pérot cavity uses a 10-cm-long Invar spacer mounted inside a temperature-controlled vacuum can. The cavity finesse is about 500, giving a cavity linewidth of about 3 MHz. The 826-nm laser is referenced to the slowly scanned cavity using a Pound-Drever-Hall locking scheme [26], giving an estimated short-term linewidth of 200 kHz at 413 nm. The vacuum can is temperature stabilized to better than 10 mK, giving a long-term frequency fluctuation of about 8 MHz at 413 nm. The combined frequency fluctuation of the two lasers, which is dominated by drift of the Invar reference cavity, is thus about 10 MHz or 0.0003 cm^{-1}.

The uncertainty in our determination of the energy of Rydberg levels is dominated by the uncertainty in our wavemeter measurement of the 413-nm laser light. The 410.5-nm MOT laser is referenced to an independent measurement of the center-of-gravity transition frequency from $4f^{11}6s^2$, $J = 15/2$ to $4f^{11}6s6p, J' = 17/2$ is obtained with a 1-m Fourier transform spectrometer calibrated against an argon line using the experimental setup described in Ref. [27]. This gives an energy of 24360.790(1) cm^{-1}, which is combined with precise measurements of the ground- [28,29] and excited-state [25] hyperfine splittings to yield an absolute frequency of the MOT laser given by 730.31682(3) THz. This value is used to calibrate the wavemeter that measures the frequency of the scanned 413-nm Rydberg laser, resulting in a total uncertainty of 200 MHz or 0.007 cm^{-1} in the absolute energy of the measured levels. Details of the energy calibration procedures are provided in the Appendix.

III. RESULTS AND DISCUSSION

From the $4f^{11}6s6p, J = 17/2$ state it is possible to excite the atom to the $4f^{11}6sns$ and $4f^{11}6snd$ Rydberg states, with a total of 12 series accessible. Due to parity conservation, the coupling to the triplet series is expected to be very weak, reducing this to the seven odd-parity singlet states $6sns(^1S_0)$, $J = 15/2$ and $6snd_{5/2,3/2}(^1D_2)$, $J = 15/2, 17/2, 19/2$ which are observed in the experiment. Figure 2 shows typical spectra for the ns and nd Rydberg series, respectively, demonstrating both the relatively narrow (∼30–60 MHz) spectral width of the technique as well as resolution of the fine-structure splitting of the nd state resonances in Fig. 2(b). As the oscillator strength decreases for higher n while the ionization rates and available dark states increase, the absolute value of the depletion is a poor indicator of absolute transition strength; however, this does provide relative strengths for closely spaced fine-structure transitions. The number of fine-structure states resolved for the nd series varies between measurements due to the finite frequency range the second photon is scanned over, but for all data sets where the full range is included, four to six states are resolved, limited by the signal-to-noise ratio for the weaker transitions.

The energy levels E_n of the Rydberg series are described by the Rydberg-Ritz formula

$$E_n = E_{\mathrm{IP}} - \frac{\mathrm{Ry}}{[n - \delta(n)]^2}, \tag{1}$$

where E_{IP} is the ionization potential which represents the series limit as $n \to \infty$ and $\delta(n)$ is the quantum defect for each series. For high-lying Rydberg states the quantum defect can be assumed to be independent of n, allowing extraction of a precision value for E_{IP} by fitting to the series convergence [11]. To verify which series the measured energy levels belong to, a Fano plot of δ modulo 1 against energy is used, as shown in Fig. 3. The measured energies then collapse into two distinct series, with the ns series having a strong series perturbation around −1.5 THz and the nd defects approximately constant for all n for each of the different fine-structure states. For the nd

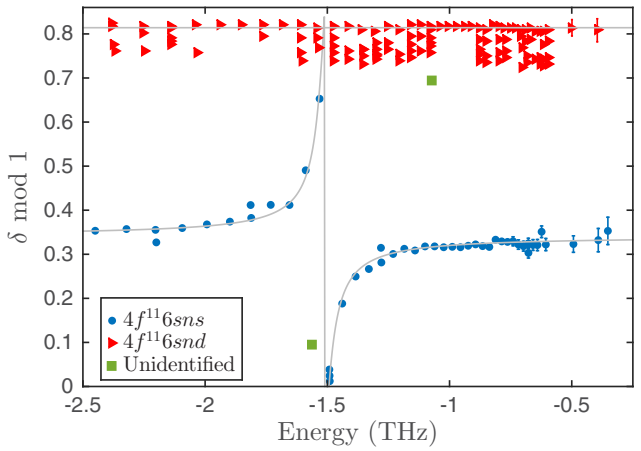

FIG. 3. (Color online) Fano plot of the quantum defect modulo 1 versus the energy of the Rydberg states. The quantum defect is constant as is expected for the d series (red triangles) and shows a perturbation at around $n = 51$ in the s series (blue circles). Green squares indicate Rydberg levels of unknown configuration. Missing fine-structure states on the nd series arise due to finite measurement ranges but have been observed for all n states measured across the $\delta = 0.7, \ldots 0.85$ range. Error bars are indicated only when larger than symbol size.

data, the series with the largest defect is typically the strongest line and has been observed across the full range of measured energies. For this reason, only this fine-structure state is used for analysis of the nd defect, as the remaining satellite states are insufficiently discriminated to clearly identify their corresponding series correctly. As the strongest dipole matrix elements are for transitions to $6snd_{5/2}(^1D_2), J = 19/2$, this is the most probable state being analyzed, from which we infer an inverted fine structure in the nd series, as is observed in the Ho^+ ionic ground state. Two additional states which could not be assigned to either ns or nd series were observed at 48530.035(7) and 48513.837(7) cm^{-1}, indicated by squares in Fig. 3.

The ionization potential is obtained using a least-squares fit to both the ns and strong nd series with $E > -1$ THz resulting in $E_{IP} = 48565.910(3)$ cm^{-1}, with both series converging to the $4f^{11}(^4I^\circ_{15/2})6s_{1/2}, J = 8$ Ho^+ ground state. The uncertainty in E_{IP} is an improvement of three orders of magnitude over previous measurements [11]. In addition to obtaining the ionization potential, this fit also yields the asymptotic values of the quantum defects corresponding to 4.324(5) and 2.814(3) for the ns and nd series, respectively. Whereas these defects are fitted modulo 1, the integer assignment is achieved by comparison to previous work [30] which predicts that the quantum defect should be ∼4.3 for the s series and ∼2.8 for the d series from the variation of δ with atomic number. This is in good agreement with the defects calculated for the known energies of the $6s^2$ and $6s5d$ states.

For lower-lying n the quantum defect can be described by the Ritz formula $\delta(n) = \delta_0 + \delta_2/(n - \delta_0)^2$ [31], which is used to fit the nd series. Unfortunately the uncertainty in δ_2 is an order of magnitude larger than the best-fit value, and the series is therefore best described by a constant defect of $\delta_0 = 2.813(3)$.

Due to the strong series perturbation in the ns series, the data cannot be described by a single-channel quantum defect model, and instead MQDT applies [32]. In this framework, the perturbation can be treated as coupling between two near-resonant series, resulting in a modification of the quantum defect of [22,32]

$$\delta(n) = \delta_0(n) - \frac{1}{\pi}\tan^{-1}\left[\frac{\Gamma/2}{(E_n - E_j)}\right], \qquad (2)$$

where Γ is the spectral width and E_j the energy of the interloper. Interestingly, despite the perturbation occurring below the first ionization potential associated with the Ho II ground state, the bound-bound series interaction can have a large spectral width comparable to a bound-continuum autoionization resonance [2].

The fitted defect is shown in Fig. 3 which accurately reproduces the observed perturbations, resulting in parameters $\delta_0 = 4.341(2), \Gamma = 6.9(3)$ GHz, and $E_j = 48515.47(4)$ cm^{-1}. The perturbing series is unknown, but likely it has the same $4f^{11}$ inner electronic configuration due to the strength of the interaction. Around this resonance the ns series is observed to split into doublets, resulting in four separate states being identified as $n = 51$ due to fine-structure splitting of the series interloper. Weak doublets are also observed for a few other s states ($n = 43,47,74$), due either to much weaker interseries resonances or potentially singlet-triplet mixing within the ns series. Above the ionization potential, we also observe a strong autoionization resonance at 48567.958(1) cm^{-1} with a FWHM of 9(1) GHz. This lies 60 GHz above the first ionization potential and thus is not an excitation to the $J = 7$

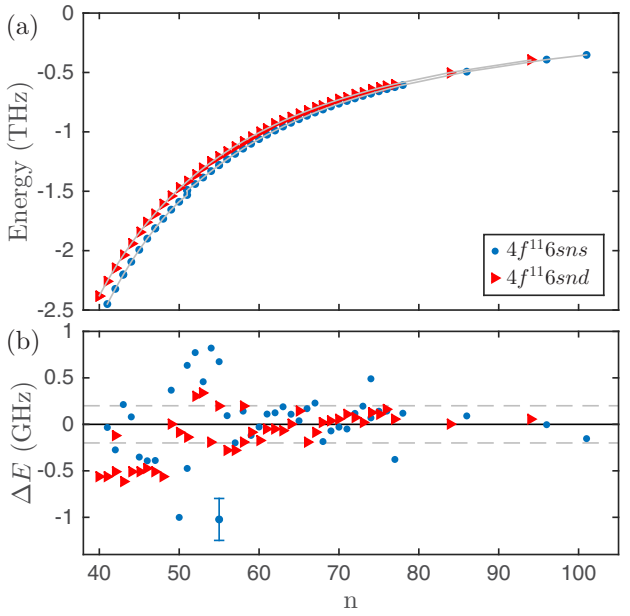

FIG. 4. (Color online) Rydberg state energy levels. (a) Measured energy levels for the ns and nd series, with solid lines calculated using fitted quantum defect parameters summarized in the text. (b) Fit residuals, yielding an rms residual of 200 MHz for $n > 60$ away from the $51s$ series perturbation, in good agreement with the 200-MHz uncertainty (indicated by the dashed gray lines and plotted as a representative error bar).

TABLE I. Measured energies for the $4f^{11}6sns$ series, accurate to 0.007 cm^{-1} with best-fit quantum defect δ determined from Eq. (2) using $\delta_0 = 4.341(2)$, $\Gamma = 6.9(3)$ GHz, and $E_j = 48515.47(4)$ cm^{-1}. The residuals relative to the Rydberg-Ritz formula are labeled ΔE. Multiple $n = 51$ states appear due to the series perturbation, as well as a number of additional weak doublets indicated by an asterisk (*).

n	Level energy (cm^{-1})	δ	ΔE (GHz)
41	48484.198	4.353	− 0.04
42	48488.466	4.355	− 0.28
43	48492.429	4.357	0.21
43	48492.537	4.357	3.46
44	48496.074	4.360	0.08
45	48499.442	4.364	− 0.36
46	48502.578	4.370	− 0.39
47	48505.407	4.377	− 2.90
47	48505.490	4.378	− 0.39
48	48508.150	4.391	− 1.68
49	48510.713	4.417	0.37
50	48512.925	4.476	− 1.00
51	48514.823	4.677	1.62
51	48516.151	4.011	− 1.75
51	48516.181	4.017	− 0.48
51	48516.207	4.022	0.63
52	48517.905	4.201	0.77
53	48519.736	4.257	0.46
54	48521.543	4.282	0.82
55	48523.194	4.294	− 1.02
55	48523.250	4.295	0.68
56	48524.853	4.302	0.10
57	48526.379	4.308	− 0.20
58	48527.843	4.312	0.15
59	48529.210	4.315	− 0.12
60	48530.516	4.317	− 0.02
61	48531.756	4.319	0.12
62	48532.929	4.320	0.13
63	48534.045	4.322	0.19
64	48535.100	4.323	0.11
65	48536.104	4.324	0.04
66	48537.066	4.324	0.17
67	48537.981	4.325	0.24
68	48538.837	4.326	− 0.18
69	48539.671	4.326	− 0.06
70	48540.465	4.327	− 0.02
71	48541.222	4.327	− 0.04
72	48541.951	4.327	0.13
73	48542.646	4.328	0.20
74	48543.305	4.328	0.08
74	48543.319	4.328	0.50
75	48543.943	4.328	0.15
76	48544.551	4.329	0.15
77	48545.118	4.329	− 0.37
78	48545.694	4.329	0.13
86	48549.460	4.331	0.10
96	48552.850	4.331	0.01
101	48554.161	4.332	− 0.14

fine-structure state of the ionic core which lies 637 cm^{-1} above E_{IP} [33].

Figure 4 shows the resulting energy residuals from the ns and nd fits, which with the exception of the increased error around the $51s$ series perturbation results in an rms residual of 200 MHz for $n > 60$, in good agreement with the 200-MHz uncertainty in determination of the absolute energy of the levels. Absolute energies and residuals for each state are given in Tables I and II, in addition to energies of the other nd fine-structure states.

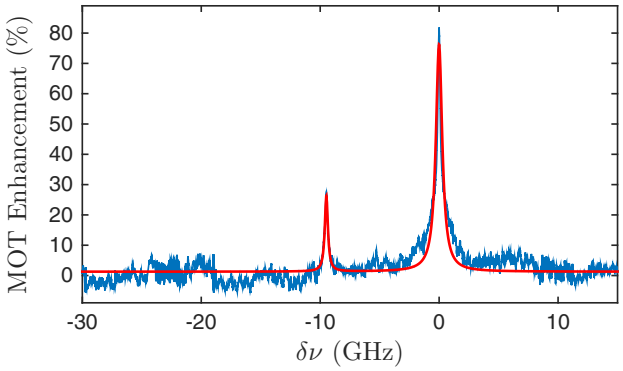

FIG. 5. (Color online) Enhancement of the MOT number as a function of detuning from $\nu = 724.2662(2)$ THz due to repumping population from a long-lived metastable state back to the ground-state cooling cycle, with a resolved hyperfine splitting of 9.47(1) GHz.

IV. MOT ENHANCEMENT RESONANCE

Alongside the depletion resonances, a strong enhancement feature was observed resulting in up to an 80% increase in the MOT atom number at $\nu = 724.2662(2)$ THz, as shown in Fig. 5. The two enhancement features have a FHWM of 600 MHz and are spaced by 9.47(1) GHz, consistent with transitions between different hyperfine states. Enhancement of the MOT arises due to repumping population either from uncoupled ground-state hyperfine levels or long-lived metastable excited states back into the $F = 11$ ground state which is cooled in the MOT. The peak enhancement wavelength is independent of the MOT detuning, verifying that this effect arises from a single photon repump transition which can be exploited to create large atomic samples. The closest matching transition from published line data is from $4f^{10}(^5I_8)5d_{5/2}6s^2, J = 17/2$ to $4f^{10}5d6s6p, J = 17/2$ [34], which has a frequency of 724.350 THz, within 10 GHz of the measured resonance.

V. SUMMARY

In summary we have measured 165 odd-parity Rydberg states belonging to the $4f^{11}6sns$ and $4f^{11}6snd$ series using MOT depletion spectroscopy, providing the first energy-resolved Rydberg spectra for neutral Ho. Analysis of the measured levels yields a significantly improved determination of the first ionization potential of $E_{IP} = 48565.910(3)$ cm^{-1}, as well as asymptotic quantum defects for the ns and nd series of 4.341(2) and 2.814(3), respectively. These data provide an important reference for testing *ab initio* theories predicting the energy levels of complex atoms. The observation of regular ns and nd series without strong perturbations for most n in the range $40 \leqslant n \leqslant 101$ suggests that we can expect to find long-lived Rydberg states suitable for creating collectively

TABLE II. Measured states for the $4f^{11}6snd$ series, accurate to 0.007 cm^{-1}. The first column represents the dominant series used for determination of the quantum defect and ionization potential for the series. The residuals relative to the Rydberg-Ritz formula are labeled ΔE, with $\delta_0 = 2.814(3)$. The remaining levels are weaker fine-structure states which could not be unambiguously assigned to a common series.

n	Energy (cm^{-1})	ΔE (GHz)	Level energies (cm^{-1})				
40	48486.532	− 0.63	48486.503	48486.720	48486.781		
41	48490.634	− 0.64	48490.700	48490.861			
42	48494.441	− 0.19	48494.428	48494.525	48494.556	48494.583	
43	48497.936	− 0.68	48498.149				
44	48501.200	− 0.57					
45	48504.231	− 0.55					
46	48507.054	− 0.52	48507.126				
47	48509.687	− 0.55					
48	48512.145	− 0.61	48512.215	48512.295	48512.344		
49	48514.466	− 0.03	48514.563				
50	48516.620	− 0.13	48516.711	48516.740	48516.782		
51	48518.643	− 0.17	48518.752	48518.789			
52	48520.560	0.28	48520.641	48520.642	48520.668	48520.702	
53	48522.351	0.32	48522.398	48522.427	48522.445	48522.452	48522.461
54	48524.019	− 0.22	48524.079	48524.107			
55	48525.622	0.17	48525.705	48525.732			
56	48527.107	−0.28	48527.144	48527.169	48527.191	48527.216	
57	48528.526	− 0.29	48528.563	48528.606			
58	48529.884	0.18	48529.871	48529.906	48529.920	48529.930	48529.949
59	48531.145	− 0.10					
60	48532.348	− 0.19					
61	48533.495	− 0.07					
62	48534.581	− 0.06					
63	48535.613	− 0.07					
64	48536.598	− 0.00	48536.624	48536.643	48536.654	48536.669	
65	48537.537	0.13	48537.562	48537.592	48537.606		
66	48538.417	− 0.20					
67	48539.270	− 0.10	48539.295	48539.321	48539.335		
68	48540.085	0.02	48540.107	48540.127	48540.139		
69	48540.860	0.03					
70	48541.601	0.04					
71	48542.310	0.10	48542.319	48542.339	48542.368		
72	48542.987	0.07	48543.005	48543.026	48543.036		
73	48543.634	0.02	48543.651				
74	48544.259	0.13	48544.297				
75	48544.854	0.11	48544.890	48544.899			
76	48545.427	0.16	48545.444	48545.461	48545.469		
77	48545.972	0.06	48545.988	48546.007	48546.015		
84	48549.261	0.00					
94	48552.714	0.05					

encoded quantum registers [9]. Determination of Rydberg lifetimes and interaction strengths will be the subject of future work. In addition to Rydberg levels, a strong repump transition has been identified, enabling a significant increase in MOT atom number. This will be useful for preparing large, dense atomic samples as a starting point for creation of a dipolar Bose-Einstein condensate [35–37] exploiting the large $9\mu_B$ magnetic moment.

ACKNOWLEDGMENT

This work was supported by funding from NSF Grant No. 1404357.

APPENDIX: ENERGY-LEVEL CALIBRATION

To provide accurate energy levels of the measured Rydberg states we use an independent measurement to determine the absolute frequency of the MOT laser, which is stabilized to the TEM_{00} mode of a high-finesse ULE cavity providing a stable long-term frequency reference. Figure 6(a) shows the relevant energy levels and splittings used in the experiment, while the laser setup is shown in Fig. 6(b). The center-of-mass frequency for the $4f^{11}6s^2\,{}^1S_0$, $J = 15/2$ to $4f^{11}6s6p\,{}^1P_1$, $J = 17/2$ transition is determined by the 1-m Fourier transform spectrometer at the National Solar Observatory using the setup detailed in Ref. [27]. High-resolution spectra from a Ho-Ar hollow cathode lamp are recorded, using lines in the well-known Ar II series [38,39] for calibration to give a

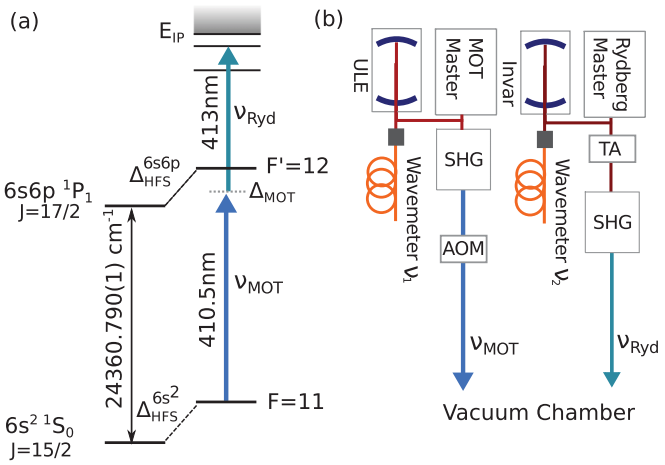

FIG. 6. (Color online) Holmium energy levels. (a) MOT and Rydberg laser transitions with respect to the ground-state energy level and hyperfine splitting. (b) Laser setup showing cavity locks, wavelength measurement, and additional frequency shift from acousto-optic modulators (AOMs) on the cooling laser. A wavemeter is used to measure the laser frequencies $\nu_{1,2}$ before they are doubled and sent to the atoms.

transition frequency of $E_{6s^2\to 6s6p} = 24360.790(1)\text{cm}^{-1}$, which is 0.02 cm^{-1} less than the value in the NIST tables [33].

For the cooling transition from $F = 11$ to $F' = 12$, the hyperfine splittings of the ground and excited states are calculated from measurements of the hyperfine constants, giving $\Delta_{F=11}^{6s^2} = 20.589319(1)$ GHz [28,29] and $\Delta_{F'=12}^{6s6p} = 19.33(1)$ GHz [25]. The frequency of the MOT transition can then be calculated from

$$\nu_{\text{MOT}} = E_{6s^2\to 6s6p} + \Delta_{F'=12}^{6s6p} - \Delta_{F=11}^{6s^2} + \Delta_{\text{MOT}}, \qquad \text{(A1)}$$

where $\Delta_{\text{MOT}} = -22(2)$ MHz is the detuning from resonance determined from spectroscopy of the atomic beam, giving $\nu_{\text{MOT}} = 730.31682(3)$ THz. Accounting for the double-pass acousto-optic modulator at 50 MHz and frequency doubling of the second-harmonic generation, the frequency of the master Ti:sapphire laser locked to the cavity is given by $\nu_{\text{ref}} = 365.15836(2)$ THz. For each measurement, the wavelength of this laser (ν_1) is recorded on a wavemeter to determine the wavemeter offset $\delta\nu = \nu_{\text{ref}} - \nu_1$. The Rydberg energy levels are then calculated from measuring the Rydberg master laser frequency (ν_2) before the doubling cavity on the same wavemeter, resulting in $\nu_{\text{Ryd}} = 2(\nu_2 + \delta\nu)$, with the absolute energy above the ground state given by

$$E_{\text{Ryd}} = \Delta_{F=11}^{6s^2} + \nu_{\text{MOT}} + \nu_{\text{Ryd}}, \qquad \text{(A2)}$$

resulting in a total uncertainty of 200 MHz on the final energy reading.

[1] T. F. Gallagher, Rep. Prog. Phys. **51**, 143 (1988).
[2] M. Aymar, C. H. Greene, and E. Luc-Koenig, Rev. Mod. Phys. **68**, 1015 (1996).
[3] M. Saffman, T. G. Walker, and K. Mølmer, Rev. Mod. Phys. **82**, 2313 (2010).
[4] M. D. Lukin, M. Fleischhauer, R. Cote, L. M. Duan, D. Jaksch, J. I. Cirac, and P. Zoller, Phys. Rev. Lett. **87**, 037901 (2001).
[5] L. Isenhower, E. Urban, X. L. Zhang, A. T. Gill, T. Henage, T. A. Johnson, T. G. Walker, and M. Saffman, Phys. Rev. Lett. **104**, 010503 (2010).
[6] T. Wilk, A. Gaëtan, C. Evellin, J. Wolters, Y. Miroshnychenko, P. Grangier, and A. Browaeys, Phys. Rev. Lett. **104**, 010502 (2010).
[7] K. Maller, M. Lichtman, T. Xia, M. Piotrowicz, A. Carr, L. Isenhower, and M. Saffman (unpublished).
[8] E. Brion, K. Mølmer, and M. Saffman, Phys. Rev. Lett. **99**, 260501 (2007).
[9] M. Saffman and K. Mølmer, Phys. Rev. A **78**, 012336 (2008).
[10] É. Biémont, Phys. Scr. **T119**, 55 (2005).
[11] E. F. Worden, R. W. Solarz, J. A. Paisner, and J. G. Conway, J. Opt. Soc. Am. **68**, 52 (1978).
[12] N. Erdmann, M. Nunnemann, K. Eberhardt, G. Herrmann, G. Huber, S. Köhler, J. Kratz, G. Passler, J. Peterson, N. Trautmann, and A. Waldek, J. Alloys Compd. **271–273**, 837 (1998).
[13] P. Xue, X. Y. Xu, W. Huang, C. B. Xu, R. C. Zhao, and X. P. Xie, AIP Conf. Proc. **388**, 299 (1997).
[14] S. G. Nakhate, M. A. N. Razvi, J. P. Connerade, and S. A. Ahmad, J. Phys. B **33**, 5191 (2000).
[15] X. Y. Xu, H. J. Zhou, W. Huang, and D. Y. Chen, Inst. Phys. Conf. Ser. **128**, 71 (1992).
[16] Y. Ogawa and O. Kujirai, J. Phys. Soc. Jpn. **68**, 428 (1999).
[17] M. Miyabe, M. Oba, and I. Wakaida, J. Phys. B **31**, 4559 (1998).
[18] T. Jayasekharan, M. A. N. Razvi, and G. L. Bhale, J. Phys. B **33**, 3123 (2000).
[19] E. Vidolova-Angelova, G. I. Bekov, L. N. Ivanov, V. Fedoseev, and A. A. Atakhadjaev, J. Phys. B **17**, 953 (1984).
[20] E. P. Vidolova-Angelova, T. B. Krustev, D. A. Angelov, and S. Mincheva, J. Phys. B **30**, 667 (1997).
[21] P. Camus, A. Débarre, and C. Morillon, J. Phys. B **13**, 1073 (1980).
[22] J. Roßnagel, S. Raeder, A. Hakimi, R. Ferrer, N. Trautmann, and K. Wendt, Phys. Rev. A **85**, 012525 (2012).
[23] E. F. Worden, L. R. Carson, S. A. Johnson, J. A. Paisner, and R. W. Solarz, J. Opt. Soc. Am. B **10**, 1998 (1993).
[24] R. W. Solarz, C. A. May, L. R. Carson, E. F. Worden, S. A. Johnson, J. A. Paisner, and J. L. J. Radzeimski, Phys. Rev. A **14**, 1129 (1976).
[25] J. Miao, J. Hostetter, G. Stratis, and M. Saffman, Phys. Rev. A **89**, 041401(R) (2014).
[26] R. W. P. Drever, J. L. Hall, F. V. Kowalski, J. Hough, G. M. Ford, A. J. Munley, and H. Ward, Appl. Phys. B **31**, 97 (1983).
[27] J. Lawler, C. Sneden, and J. J. Cowan, Astrophys. J. Lett. **604**, 850 (2004).
[28] W. Dankwort, J. Ferch, and H. Gebauer, Z. Phys. A **267**, 229 (1974).
[29] B. Burghardt, S. Büttgenbach, N. Glaeser, R. Harzer, G. Meisel, B. Roski, and F. Träber, Z. Phys. A **307**, 193 (1982).

[30] U. Fano, C. E. Theodosiou, and J. L. Dehmer, Rev. Mod. Phys. **48**, 49 (1976).
[31] W. Ritz, Ann. Phys. (Berlin) **317**, 264 (1903).
[32] M. J. Seaton, Rep. Prog. Phys. **46**, 167 (1983).
[33] W. C. Martin, R. Zalubas, and L. Hagan, Natl. Stand. Ref. Data Ser. **60**, 296 (1978).
[34] S. Kröger, J.-F. Wyart, and P. Luc, Phys. Scr. **55**, 579 (1997).
[35] T. Lahaye, C. Menotti, L. Santos, M. Lewenstein, and T. Pfau, Rep. Prog. Phys. **72**, 126401 (2009).
[36] M. Lu, N. Q. Burdick, S. H. Youn, and B. L. Lev, Phys. Rev. Lett. **107**, 190401 (2011).
[37] K. Aikawa, A. Frisch, M. Mark, S. Baier, A. Rietzler, R. Grimm, and F. Ferlaino, Phys. Rev. Lett. **108**, 210401 (2012).
[38] R. C. M. Learner and A. P. Thorne, J. Opt. Soc. Am. B **5**, 2045 (1988).
[39] W. Whaling, W. H. C. Anderson, M. T. Carle, J. W. Brualt, and H. A. Zarem, J. Res. Natl. Inst. Stand. Technol. **107**, 149 (2002).